

KATEDRA FIZYKI ZJAWISK ELEKTRONOWYCH

Laboratorium

Metody Badań Spektroskopowych

Wyznaczanie stałych spektroskopowych
stanów wzbudzonych
cząsteczki azotu

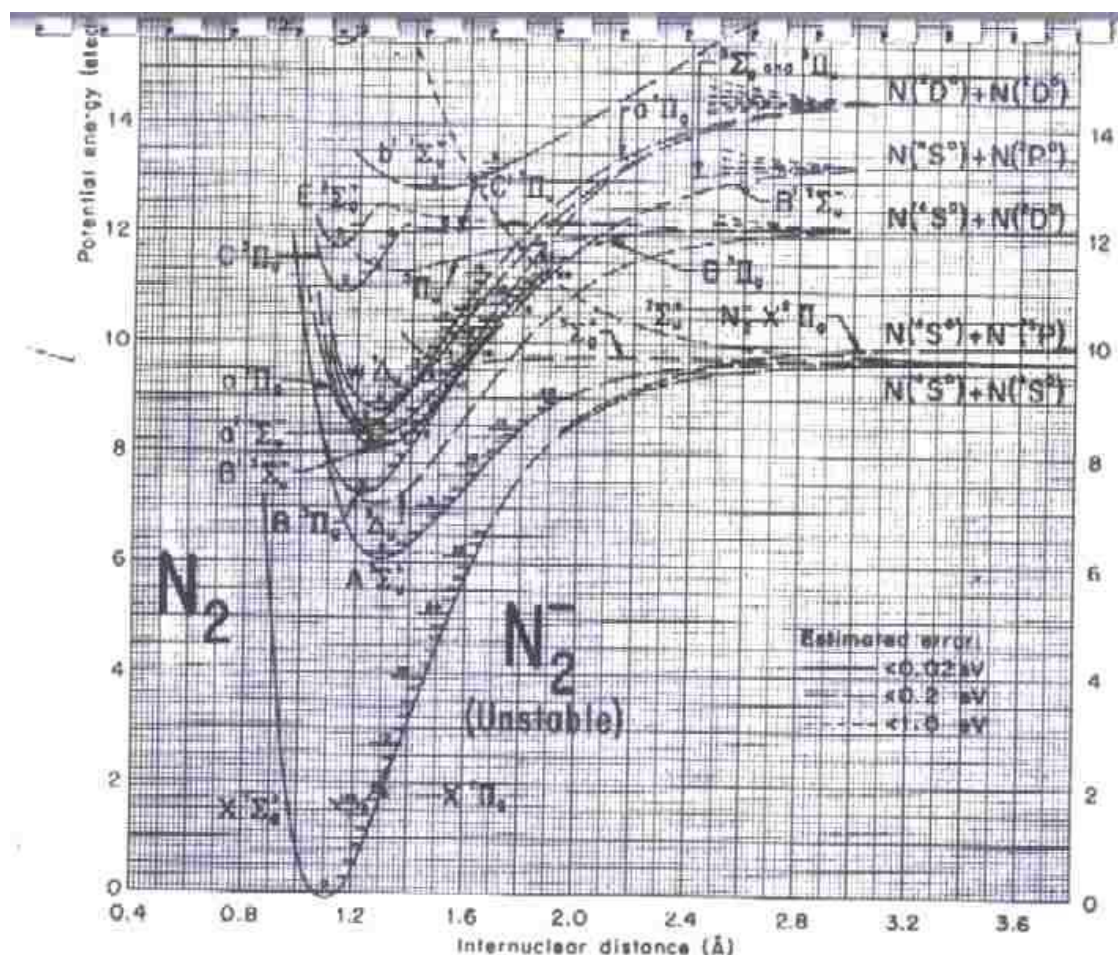


Wyznaczanie stałych spektroskopowych stanów wzbudzonych cząsteczki azotu

ZADANIA:

1. Wykonać pomiar widma fluorescencji azotu.
2. Wykonać pomiar funkcji wzbudzenia poziomu oscylacyjnego $v=0$ stanu $C^3\Pi_u$.
3. Wyznaczyć długość fali obserwowanych linii widmowych.
4. Wyznaczyć stałe spektroskopowe $\bar{\omega}_e$, $x_e\bar{\omega}_e$ stanów wzbudzonych $C^3\Pi_u$ i $B^3\Pi_g$ cząsteczki azotu.
5. Wyznaczyć krzywe energii potencjalnej stanów $C^3\Pi_u$ i $B^3\Pi_g$.
6. Przeprowadzić dyskusję otrzymanych wyników.

DODATEK A: Krzywe energii potencjalnej cząsteczki azotu



DODATEK B: Charakterystyka trochoidalnego monochromatora elektronów.
 Stamatovic, Schulz, *Rev. Sci. Instrum* **41**, 423 (1970)

THE REVIEW OF SCIENTIFIC INSTRUMENTS VOLUME 41, NUMBER 3 MARCH 1970

Characteristics of the Trochoidal Electron Monochromator*

A. STAMATOVIC† AND G. J. SCHULZ
 Mason Laboratory, Yale University, New Haven, Connecticut 06520
 (Received 9 September 1969)

An electron monochromator for use in an axial magnetic field is described. Electrons are injected parallel to the magnetic field and an electric field is applied in a perpendicular direction. The electrons thus describe trochoids and drift in a direction perpendicular to both the electric and magnetic fields and disperse according to their initial velocities. An electron energy width at half-maximum of 0.020 eV can be obtained, with a transmitted current of about 10^{-8} A.

INTRODUCTION

IN many studies of electron interaction with atoms, molecules, and surfaces, particularly at low electron energies, it is desirable to produce a beam of monoenergetic electrons in an axial magnetic field. The axial magnetic field prevents spreading of the electron beam and allows separation of electrons and negative ions. In the ion source of a mass spectrometer, the magnetic field prevents changes in the shape of the electron beam with change of electron energy and thus provides extraction conditions which are independent of electron energy.

The most common method for reducing the energy spread of electrons in an axial magnetic field is the retarding potential difference method, developed by Fox *et al.*¹ In this method, electrons are retarded at one of the electrodes of the gun so as to create an energy distribution with a sharp low energy cutoff. The cutoff potential is changed by a small amount and the difference in signal current is measured. Generally, one can obtain a width at half-maximum of the energy distribution of about 0.1 eV. The noise on a difference signal is the result of the noise in the total transmitted electron current, rather than the difference electron current. Thus, noise is often undesirably large when the retarding potential difference method is used.² A mathematical analysis of the retarding potential difference method is given by Anderson *et al.*³⁻⁵

The choice of other electron monochromators suitable for use in the presence of an axial magnetic field is very limited. In fact, it seems that the only other method is that described by Hartl⁶ in which an electrostatic lens with high chromatic aberration is used as an energy dispersive element. The use of very high voltages in this type of monochromator and the strong dependence on the value of the magnetic field do not seem convenient for the study of low energy electron collisions with atoms and molecules.

The trochoidal electron monochromator, described in this paper, overcomes the noise problem of the retarding potential difference method and gives, without the use of high voltages, an energy distribution with a full width at half-maximum of about 0.02 eV. The theory of operation, design problems, and results obtained with the trochoidal electron monochromator are discussed in this paper.

I. PRINCIPLE OF OPERATION

The field configuration used in the trochoidal electron monochromator has been briefly described by us in a previous communication⁷ and is shown in Fig. 1. Electrons enter the monochromator along the Z axis, i.e., parallel to the magnetic field, and an electric field is applied along the Y axis. Such a field configuration has been used by Bleakney and Hipple⁸ in a mass spectrometry, and by Bailey⁹ and Barr and Perkins¹⁰ for an analysis of charged particles emanating from a plasma. This field configuration differs from that of a Wien filter,¹¹ in which the incident electron beam direction is perpendicular both to the electric and the magnetic field directions.

The motion of charged particles in the configuration of

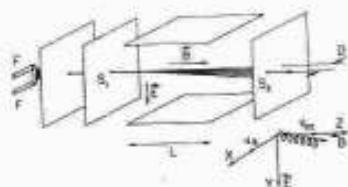


FIG. 1. Schematic diagram of the field configuration used for the trochoidal monochromator.

fields that exists in the trochoidal electron monochromator is described in papers⁸⁻¹⁰ as well as in textbooks.¹²⁻¹⁴ Therefore, only a simple procedure for following the particle motion¹² will be given in this paper.

The equation of motion of an electron in crossed electrostatic and magnetic fields is given by

$$d\mathbf{v}_0/dt = -(e/m)[\mathbf{E} + (\mathbf{v}_0 \times \mathbf{B})], \quad (1)$$

where \mathbf{v}_0 is the incident electron velocity, e and m are the charge and the mass of the electron, respectively, while \mathbf{E} is the electric field, and \mathbf{B} is the magnetic field. The configuration of fields given in Fig. 1 has no force component acting in the direction of the magnetic field, i.e., in the direction of the incident electron beam. The velocities of the electrons along the Z axis are therefore uniform. This allows us to introduce a set of moving coordinates which move in the direction of the X axis with velocity given by

$$\mathbf{v}_d = (\mathbf{E} \times \mathbf{B})/B^2. \quad (2)$$

The velocity in the moving coordinate system is related to the velocity in the stationary coordinate system by the relations,

$$\mathbf{v}_0(x, y) = \mathbf{v}_d + \mathbf{v}(x', y'); \quad d\mathbf{v}_0(x, y)/dt = d\mathbf{v}(x', y')/dt, \quad (3)$$

where $\mathbf{v}_0(x, y)$ is a component of incident velocity in the X-Y plane, and $\mathbf{v}(x', y')$ is the corresponding component of incident electron velocity in the moving set of coordinates. Substituting Eqs. (2) and (3) into Eq. (1) gives the equation for the motion of electrons in the moving coordinate system,

$$d\mathbf{v}(x', y')/dt = -(e/m)[\mathbf{v}(x', y') \times \mathbf{B}]. \quad (4)$$

This represents a circular motion with radius ρ and angular velocity ω ,

$$\rho = mv(x', y')/(eB), \quad \omega = eB/m. \quad (5)$$

The use of a moving set of coordinates, with the velocity given by Eq. (2), eliminates the electric field from the equation for electron motion. The combination of the circular motion in the moving set of coordinates and the motion of the moving coordinate system itself gives as a projection of the electron motion on the X-Y plane one of several types of trochoids. The type of trochoid depends on the relation of the incident electron velocity vector to the magnetic field direction. In all these cases the electrons are deflected in the direction perpendicular to both the magnetic and the electric fields, and after passing through the crossed-field region they move in the magnetic field direction, but are displaced from the previous axis (see Fig. 1). The amount of displacement depends on the number of trochoids completed by the electrons during their stay in the crossed-field region; i.e., on their velocity component in the Z-axis direction. Thus the energy selection in this monochromator occurs as a result of the time

of flight of the electrons. The displacement from the axis, D , is given by

$$D = v_d t, \quad (6)$$

where t is the time spent by the electrons in the crossed-field region and can be written as

$$t = L/v_{0z} = L(2w/m)^{-1/2}. \quad (7)$$

Here v_{0z} is the initial velocity along the Z direction, $w = \frac{1}{2} m v_{0z}^2$, and L is the length of the crossed-field region.

Combining Eqs. (6) and (7) we obtain

$$D = v_d L / v_{0z} = v_d L (2w/m)^{-1/2}. \quad (8)$$

By partial differentiation of Eq. (8) we obtain the energy spread Δw ,

$$\Delta w/w = 2\Delta D/D, \quad (9)$$

where ΔD is the sum of the aperture diameters of the entrance and exit electrodes ($\Delta D = S_1 + S_2$).

The optimum energy spread is obtained for the lowest values of w . Thus one wishes to operate the monochromator at very low electron energies. This is achieved in the present device by retarding the electrons in the deflection region. This retarding field also rejects most of those electrons whose velocity vector is not oriented axially.

An additional energy spread results from the transverse electric field. The maximum potential drop across the electron beam is ES_1 , where S_1 is the diameter of the entrance aperture. This potential drop causes a velocity spread in the analyzer and thus adds to the energy distribution.

Combining Eqs. (2), (8), and (9), and adding the potential drop across the electron beam, we obtain the following expression for the full width at the base of the energy distribution at the exit of the monochromator:

$$\Delta w = E^2 L^2 m \Delta D / (B^2 D^2) + eES_1. \quad (10)$$

The full width at half-maximum, which is the quantity measured experimentally, is of course smaller. Simpson¹³ concludes that the ratio of the base width to the half-width, $(\Delta w/\Delta w_{1/2})$, is equal to 2 for a well designed instrument. Hayward¹⁴ finds that this ratio is 2.4 for a 180° magnetic analyzer. We find from experiment that for the presently used trochoidal monochromator this ratio is 2.5-3.5.

II. DESCRIPTION OF THE MONOCHROMATOR AND OPERATION

The electrode arrangement of the monochromator is shown in Fig. 2. The electron source consists of a hairpin-shaped thorium-coated iridium filament and is followed by three electrodes P_1 , P_2 , and P_3 , the last of which serves as the entrance electrode into the crossed field region. The deflector plates D_1 and D_2 are made by machining a cylinder of the same diameter as the electrode disks and by

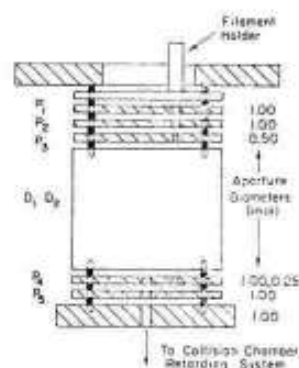


Fig. 2. Diagram of the electrode arrangement of the monochromator. The approximate operating potentials, referred to the filament center, are as follows: P_1 (1 V), P_2 (5 V), P_3 (0.3 V), the mid-plane of the deflection field (less than 0.1 V), P_4 (less than 0.1 V), P_5 (1.5 V). The potentials of electrodes P_2 - P_5 are adjusted for maximum electron current into the monochromator, while the other potentials are adjusted for the best possible energy distribution in the transmitted electron beam. The spacing between electrodes is approximately 1 mm and the spacing between deflection plates (D_1 - D_2) is 3.2 mm.

cutting it in half along its axis. The spacing between the two parallel surfaces of the deflector is about 0.32 cm. The electrodes P_1 - P_3 are disks 1.6 cm in diameter and 0.15 cm thick, made of Advance, a nonmagnetic alloy of copper and nickel. Each electrode, as well as the deflector plates, has six holes (0.12 cm diam), equally spaced on a 1.27 cm diam circle. These holes serve as seats for sapphire balls (0.151 cm diam), which are used as spacers and insulators between electrodes. All electrodes, the deflector, and the filament holder are held together by two end plates and four bolts joining the lower and the upper end plates.

Three sets of deflector plates with lengths of 0.63, 1.27, and 1.90 cm have been used, with the last one giving the best results. The sizes of the electron beam apertures are given in Fig. 2. The filament and the apertures on electrodes P_1 , P_2 , and P_3 are displaced by 0.32 cm from the axis, whereas the exit and all subsequent electrodes have their holes on the axis of the monochromator. The exit aperture is funnel shaped to prevent reflection of electrons from the aperture walls. The off-center aperture on the exit electrode P_4 is used for alignment of the magnetic field. With the deflection field switched off, the magnetic field is aligned by maximizing the electron current to electrode P_5 . All electrodes are gold plated and the high vacuum part of the system is baked to minimize contact potentials.

The electron energy distribution is determined in two ways; namely, by taking the derivative of a retarding curve and by measuring the negative-ion current resulting from electron attachment⁷ in SF_6 . The latter is made possible by adding a collision chamber with an ion collector between the monochromator and the retarding system. The retarding system consists of three electrodes which are kept at the same potential in order to ensure a homogene-

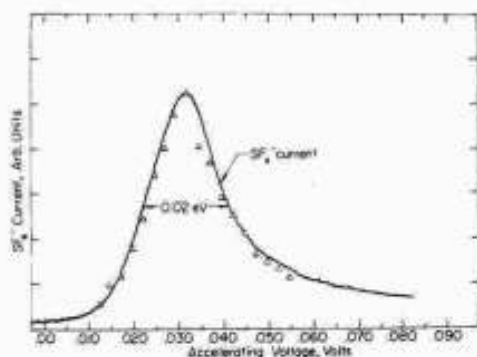


FIG. 3. The shape of the electron energy distribution. The full line is the energy dependence of the SF_6^- ion current measured in the collision chamber. The triangular points are obtained by taking the derivative of the electron beam retarding curve and normalizing to the peak of the SF_6^- current.

ous electrostatic field in the space where retarding is occurring. Figure 3 shows the electron energy distribution obtained by these two methods and it is seen that the two methods agree well. The full width at half-maximum of the energy distribution is about 0.02 eV. The energy spread at the base of the energy distribution curve is about 2.5–3.5 times larger than at half-maximum. The current that can be obtained with this energy distribution is about 10^{-4} A.

III. CHARACTERISTICS OF THE MONOCHROMATOR

The width of electron energy distribution in a given geometry and in a fixed magnetic field depends on the

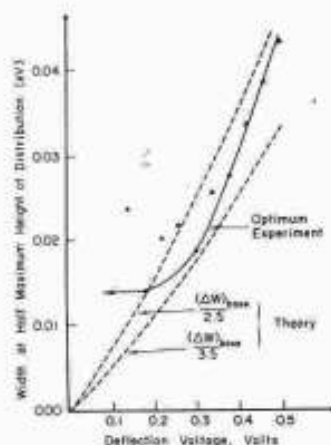


FIG. 4. Characteristics of the monochromator at $B=100$ G. The triangular points correspond to the experimental width at half-maximum vs the deflection voltage U applied between D_1 and D_2 . The solid line is drawn through the lowest lying experimental points and represents the "optimum" curve. The dashed lines are obtained by dividing values obtained from Eq. (10), which correspond to the full width at the base, by a factor 2.5 and 3.5, respectively. By this division we approximate the theoretical values for the width at half-maximum of the energy distribution.

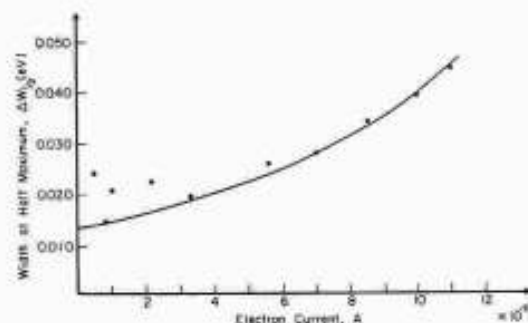


FIG. 5. The relationship between the width at half-maximum of the electron energy distribution and the maximum electron beam current.

deflection voltage, as shown in Eq. (10). Figure 4 shows the dependence of the width of the electron energy distribution on deflection voltage. The points are experimental determinations of the width at half-maximum. The solid curve is drawn through the experimental points which show the lowest half-width, and thus should be considered as the "optimum" experimental curve. It is believed that the large departure of some of the experimental points from the optimum curve is caused by the passage through the exit aperture of secondary electrons which are reflected from monochromator surfaces. This effect is especially pronounced at those values of the deflection voltage for which the trajectories of the secondary electrons pass the exit aperture.

Also shown in Fig. 4 are plots of Δw obtained from Eq. (10), but reduced by a factor of 2.5 and 3.5. This reduction factor approximates the ratio of the width at the base of the distribution and the width at half-maximum.

The influence of reflected electrons on the energy distribution was checked by plating the monochromator electrodes with platinum black in order to decrease the reflection coefficient for low energy electrons. This reflection coefficient is about 80% for gold plated surfaces, and about 30% for platinum-black-coated surfaces.¹⁷ A significant decrease in the width of the energy distribution was ob-

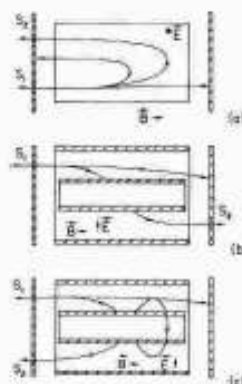


FIG. 6. Other possible field geometries similar to the trochoidal electron monochromator.

served when the electrodes were coated with platinum black.

A search for space charge effects in the monochromator shows that space charge effects become important at relatively high electron currents only at the entrance aperture of the monochromator. In the region of the deflector electrodes, dispersion of the electron beam takes place and thus the current density is lower than in the region of the entrance electrode.

Figure 5 shows the relationship between the measured width at half-maximum and the electron beam current that can be transmitted through the monochromator. The operating voltages are adjusted, in this case, for maximum electron current at a given half-width. When the magnetic field is increased (up to 250 G), the transmitted electron current also increases, but the effect on the energy distribution is not very large. Table I shows the experimental relations between the magnetic field, transmitted electron current, and the width at half-maximum of the electron energy distribution. The first three rows of data are taken at constant E/B .

IV. OTHER GEOMETRIES

Figure 6 shows geometries which are similar to that discussed in the previous sections, but which may be advantageous in some applications. It is expected that the monochromators shown in Fig. 6 will have similar characteristics. In Fig. 6(a) is shown a geometry in which electrons enter the deflector region through aperture S_1 , are turned by 180° in the deflector region, and exit through aperture S_2 . A preliminary check using such a monochromator shows that the characteristics are similar to those shown in Fig. 3. Figures 6(b) and (c) show geometries in which the electric field is created by application of voltages between cylinders. Although the latter designs are expected

TABLE I. The experimental relations between the magnetic field B , the deflection voltage U , transmitted electron current I_e , and the experimental width at half-maximum of the electron energy distribution $(\Delta w)_{1/2}$.

B	U	I_e	$(\Delta w)_{1/2}$
100 G	0.120 V	1.2×10^{-8} A	0.018 eV
150	0.175	1.8×10^{-8}	0.020
200	0.240	3.4×10^{-8}	0.021
250	0.340	5.7×10^{-8}	0.026

to exhibit high dispersion, the construction appears to be difficult.

The authors are grateful to I. B. Bernstein, P. D. Burrow, M. J. W. Boness, and D. Spence for many very helpful discussions and advice. Thanks are due to J. H. Kearney for invaluable assistance in the design.

* This work has been supported by DASA through ARO-D and by the National Science Foundation.

† Permanent address, Institute of Physics, P.O. Box 57, Belgrade, Yugoslavia.

¹ R. E. Fox, W. M. Hickam, D. J. Grove, and T. Kjeldnaas, Jr., *Rev. Sci. Instrum.* **26**, 1101 (1955).

² P. Marmet, *Can. J. Phys.* **42**, 2102 (1964).

³ N. Anderson, P. P. Eggleton, *Int. J. Electron.* **22**, 497 (1967).

⁴ N. Anderson, P. P. Eggleton, and R. G. W. Keesing, *Rev. Sci. Instrum.* **38**, 924 (1967).

⁵ N. Anderson, P. P. Eggleton, *Rev. Sci. Instrum.* **38**, 1524 (1967).

⁶ W. A. M. Hartl, *Z. Physik*, **191**, 487 (1966).

⁷ A. Stamatovic and G. J. Schulz, *Rev. Sci. Instrum.* **39**, 1752 (1968).

⁸ W. Bleakney and J. A. Hipple, Jr., *Phys. Rev.* **53**, 521 (1938).

⁹ L. Evan Bailey, *Rev. Sci. Instrum.* **31**, 1147 (1960).

¹⁰ W. L. Barr and W. A. Perkins, *Rev. Sci. Instrum.* **37**, 1354 (1966).

¹¹ H. Boersch, J. Geiger, and W. Stöckel, *Z. Physik* **180**, 415 (1964).

¹² L. Page and N. I. Adams, Jr., *Principles of Electricity*, (D. Van Nostrand Company, Inc. New York, 1952), pp. 272-276.

¹³ H. S. W. Massey and H. Kestelman, *Ancillary Mathematics*, (Sir Isaac Pitman and Sons, Ltd., London, 1959), pp. 722-724.

¹⁴ J. R. Pierce, *Theory and Design of Electron Beams*, (D. Van Nostrand Company, Inc., New York, 1954), pp. 26-28.

¹⁵ J. A. Simpson in *Methods of Experimental Physics*, L. Marton, ed., (Academic Press Inc., New York, 1967), Vol. 4A, p. 129.

¹⁶ R. W. Hayward, *Advan. Electron.* **5**, 104 (1953).

¹⁷ P. Marmet and L. Kerwin, *Can. J. Phys.* **38**, 787 (1960).